symmetry

MDPI

Article

New Schiff Base–TMB Hybrids: Design, Synthesis and Antiproliferative Investigation as Potential Anticancer Agents

Najiah M. Alyamani

Department of Biology, College of Science, University of Jeddah, Jeddah 21493, Saudi Arabia; nmalyamani@uj.edu.sa

Abstract: The structural symmetry or asymmetry of organic compounds is one of the most fundamental characteristics. *Z*-geometrical isomers are promiscuous and kinetically preferred structures with a plethora of biological activities. A new series of hybrid molecules containing Schiff base and 3,4,5-trimethoxybenzamide moieties were synthesized from the starting material ethyl acrylate ester derivative (***Z***)-**1** and structurally confirmed by elemental microanalysis, ^{1}H-NMR, and ^{13}C-NMR spectroscopic studies. The in vitro cytotoxic activity of the target hybrids was tested against the MCF-7 breast cancer line compared with colchicine as the reference compound. Most of the newly synthesized hybrids showed good growth inhibition activity against the MCF-7 cells compared to the reference substance. The results of the β-tubulin polymerization inhibition activity assay showed that the *p*-vanillin Schiff base **4g** displayed good inhibition activity. In addition, *p*-vanillin Schiff base **4g** exhibited antiproliferative activity over the MCF-7 cells by cellular cycle blockade at the G2/M phase and it is a potent apoptotic agent. qRT-PCR analysis showed that Schiff base **4g** boosted the mRNA expression of the p53 and Bax levels while lowering the expression of the Bcl-2 level.

Keywords: Schiff base; trimethoxybenzamide; cytotoxicity; tubulin; cell cycle analysis; mRNA expression

Citation: Alyamani, N.M. New Schiff Base–TMB Hybrids: Design, Synthesis and Antiproliferative Investigation as Potential Anticancer Agents. *Symmetry* **2023**, *15*, 609. https://doi.org/10.3390/sym15030609

Academic Editor: George Papageorgiou

Received: 31 January 2023
Revised: 18 February 2023
Accepted: 21 February 2023
Published: 28 February 2023

1. Introduction

Breast cancer is one of the most prevalent female malignancies in the world [1,2]. Advances in biochemistry diagnosis, especially in breast specific screening, have resulted in an early stage of breast cancer [3]. Breast cancer cells have a high mitotic rate due to excess microtubule formation [4]. Antimitotic drugs are a major class of anticancer agents that are very useful in the treatment of cancer [5]. The target of these agents is tubulin, a heterodimer protein formed from the α and β subunits [6]. Dimers of α and β-tubulin polymerize to form microtubules [7]. During cellular division, microtubules play a crucial function as the key component of the mitotic spindle to ensure proper chromosome segregation [8]. Aside from mitosis, microtubules are also involved in cellular transport, the regulation and maintenance of cell morphogenesis, and many other important physiological functions [9,10]. Hindering of the proper function and/or formation of the microtubules result in the disruption of cellular division in the G2/M phase, and subsequently, cellular apoptosis [11,12]. Many natural antimitotic molecules target the mitotic process such as colchicine **I**, combretastatin A-4 (CA-4) **II**, vinca alkaloids, and taxans [13–15]. It has been demonstrated that some *Z*-configurated isomers substituted on the trimethoxy phenyl (TMP) or trimethoxybenzamide (TMB) moieties possess cytotoxic and antimitotic activity due to their ability to inhibit tubulin polymerization [16,17]. These isomers work by binding to the colchicine binding site to provide that effect [18].

Apoptosis is an active brake for abnormal and damaged cells [19]. Breast cancer progression and the development of chemotherapeutic resistant breast cancer have been linked to a number of genetic and epigenetic anomalies, among which is the inhibition of apoptotic pathways [20,21]. The high expression of anti-apoptotic protein Bcl-2 and low levels of Bax expression have been correlated to the poor therapeutic response of breast

cancer cells in traditional therapies [22,23]. Therefore, apoptosis induction in cancer cells via targeting one or more of the key enzymes of apoptosis in cancer cells such as Bcl-2 and Bax appear to be attractive for breast cancer patients [24,25].

Structural symmetry and asymmetry are one of many contributing aspects that must be taken into account when designing biologically active molecules. Schiff bases represent an important pharmacophore for many bioactive agents with a pronounced anticancer effect [26]. A plethora of Schiff base-containing derivatives have been reported to possess cytotoxic activity against different cancer cell lines [27–29]. Schiff base **III** is open chain linkers of CA-4 and displays potent β-tubulin polymerization inhibition activity [30] (Figure 1). The TMB group has been widely applied in pharmaceuticals due to its unique structural and physicochemical characteristics [31,32]. TMB-containing compounds exhibit various biological activities including anticancer activity [33]. Many TMB derivatives have been stated for their cytotoxic effect via the inhibition of tubulin polymerization [34]. For example, trimethoxybenzamide molecule **IV** was evaluated as an inhibitor of β-tubulin polymerization with significant antiproliferative activity against MDA-MB-231 breast cancer cells with IC_{50} = 1.27 μM [17], Figure 1. It was also reported that 4-(dimethylamino)phenyl-containing derivatives demonstrate cytotoxic activities against several cancer cell lines [35–37].

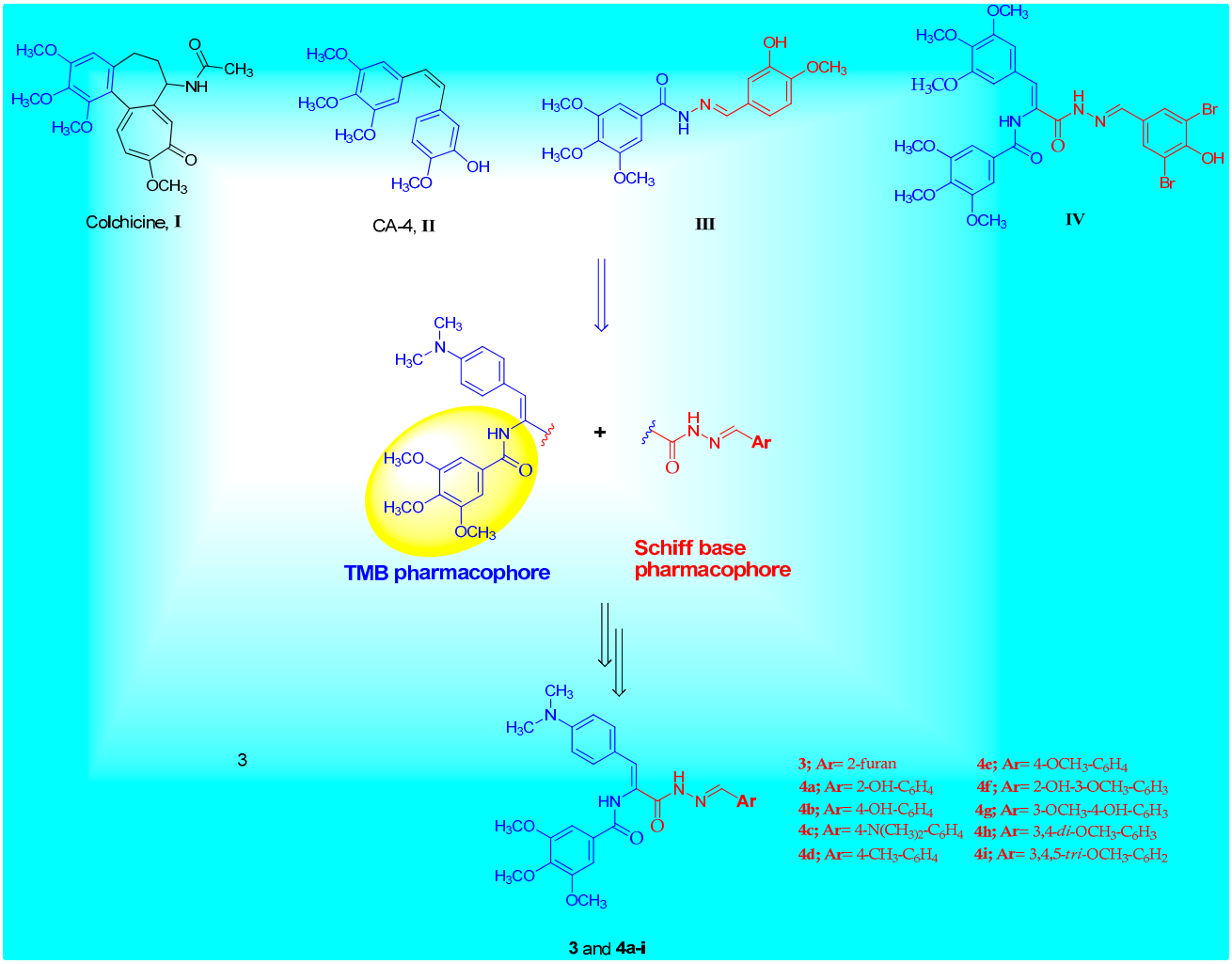

Figure 1. The chemical structures of colchicine **I**, CA-4 **II**, structurally related tubulin polymerization inhibitors **III, IV** and the general structure of the target Schiff base–TMB molecules **3** and **4a–i**.

Encouraged by the aforementioned aspects, the objective of the current work was to synthesize a hybrid series of Schiff base derivatives containing TMB moiety. In addition, the TMB group is attached to the (*Z*)-4-(dimethylamino)phenyl function. These prepared Schiff base derivatives underwent screening for their in vitro cytotoxic activity against the MCF-7 breast cancer cell line. After that, further molecule mechanistic investigations of the anticancer activity were carried out for the most potent molecules. Therefore, *p*-vanillin Schiff base **4g** was chosen to perform extra investigations such as the tubulin polymerization inhibition assay, cell cycle analysis, and apoptosis related studies.

2. Results and Discussion

2.1. Chemistry

The synthetic pathways applied in the synthesis of the target Schiff base–TMB molecules **3** and **4a–i** are illustrated in Scheme 1. In the present work, the key starting material **(*Z*)-1** was prepared through the reaction of appropriate oxazolone in refluxing absolute ethanol in the presence of triethylamine (Et_3N), as reported [38]. The key starting material **(*Z*)-1** was reacted with hydrazine hydrate in an ethanolic solution to afford the hydrazide intermediate **(*Z*)-2** [39]. The chemical structure of the hydrazide intermediate **(*Z*)-2** was elucidated based on the ^{1}H-NMR and ^{13}C-NMR spectral studies. The ^{1}H-NMR spectrum of the hydrazide molecule **(*Z*)-2** was characterized by the presence of two NH proton signals at δ 9.75 and 9.28 ppm along with the presence of a signal at δ 4.34 ppm attributed to the amino (NH_2) protons. Moreover, the aromatic ring protons of the key hydrazide **(*Z*)-2** displayed a characteristic doublet of doublet signals at δ 7.44 and 6.67 ppm integrating four protons, which corresponded to the phenyl protons of the 4-*N*,*N*-dimethylphenyl ring as well as a singlet signal at δ 7.40 ppm, which was attributed to two phenyl protons of the trimethoxyphenyl moiety. In addition, at δ 7.16 ppm, the olefinic proton showed up as a singlet signal. The ^{13}C-NMR spectrum of the hydrazide **(*Z*)-2** displayed two signals at δ 165.69 and 165.52 ppm corresponding to two carbonyl (C=O) carbons. Furthermore, the key hydrazide **(*Z*)-2** exhibited sets of three aliphatic signals as follows: methoxy carbon (OCH_3) at δ 60.56 ppm, two methoxy carbons ($2OCH_3$) at δ 56.51 ppm, and *N*,*N*-dimethyl carbons ($(CH_3)_2N$) at δ 40.15 ppm. The target Schiff base–TMB hybrids **3** and **4a–i** were prepared by reacting the key hydrazide intermediate **(*Z*)-2** with furfural or the respective aryl aldehyde in an ethanolic solution, catalyzed with glacial acetic acid [39]. The new Schiff base–TMB hybrids were clarified by the ^{1}H-NMR and ^{13}C-NMR spectral studies and their purity was established by microanalyses. The ^{1}H-NMR spectrum of furfural Schiff base **3** in DMSO-d_6, as a representative example, elicited three singlet signals at δ 11.42, 9.87, and 8.32 ppm characteristic for two NH and azomethine (HC=N) protons, respectively. The three methine protons of the furan ring showed a peak at δ 7.83 ppm as a singlet signal, at δ 6.87 ppm as a doublet signal and at δ 6.65–6.60 ppm as a multiplet signal. In addition, the ^{1}H-NMR spectra of compound **3** showed the presence of three peaks at δ 3.87, 3.75, and 2.94 ppm, integrating the trimethoxy ($3OCH_3$) and *N*,*N*-dimethyl ($(CH_3)_2N$) protons, respectively. Furthermore, in the ^{1}H-NMR spectrum of **3**, a signal arising from the NH_2 protons of the parent compound at δ 4.43 ppm was not observed. This finding also supports the structure of 3,4,5-trimetoxybenzamido-Schiff base **3**. The ^{13}C-NMR spectrum of **3** displayed two signals at δ 165.60 and 162.94 ppm, assignable to the two carbonyl carbon (2C=O). The ^{13}C-NMR spectrum of compound 3 showed a resonance of azomethine carbon (HC=N) at δ 145.39 ppm. Furthermore, the furfural Schiff base–TMB **3** showed the detection of three signals at δ 60.59, 56.55, and 40.14 ppm due to the presence of trimethoxy ($3OCH_3$) and *N*,*N*-dimethyl carbons($(CH_3)_2N$), respectively.

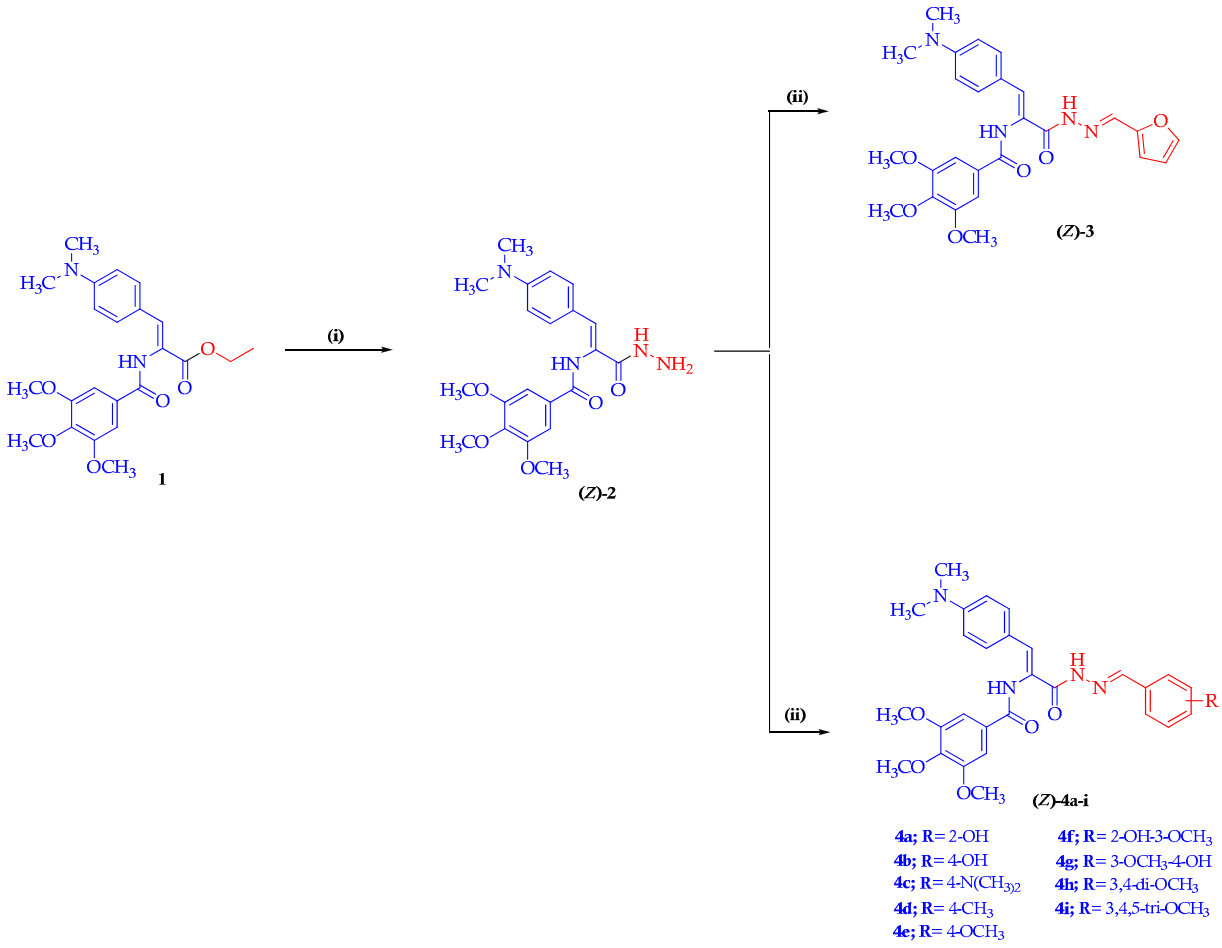

Scheme 1. Representative synthetic routes for the target Schiff base–TMB derivatives **3** and **4a–i**. Reagents and reaction condition: (**i**) hydrazine hydrate, EtOH, reflux 4h; (**ii**) furfural or respective aryl aldehyde, EtOH, AcOH, reflux 6–8 h.

2.2. Biology

2.2.1. Cytotoxic Activity against the MCF-7 Breast Cancer Cell Line

To determine the IC_{50}, the prepared Schiff base–TMB hybrids **3** and **4a–i** were analyzed using the standard colorimetric MTT test on the breast cancer cell line MCF-7. In the current investigation, colchicine (Col) was used as the positive reference control. The in vitro cytotoxicity screening results showed that the tested Schiff base–TMB molecules showed a significant antiproliferative activity against the MCF-7 breast cancer cells (Table 1). *p*-Hydroxybenzaldehyde Schiff base **4b**, *o*-vanillin Schiff base **4f**, and *p*-vanillin Schiff bas **4g** showed 1,3-, 1.4-, and 2.5-fold, respectively, more potent cytotoxic activity than Col. On the basis of the obtained IC_{50} values against the MCF-7 breast cancer cells, compounds **4b**, **4f**, and **4g** displayed a higher cytotoxic activity with IC_{50} values 4.74, 4.01, and 2.28 µM, respectively, compared with col (IC_{50} = 5.74 µM). Furthermore, *p*-vanillin Schiff bas **4g** was further tested for its cytotoxic effects against the normal breast cell line MCF-10A. The results showed a selective mode of cytotoxic activity with an IC_{50} value of 26.84 µM.

2.2.2. β-Tubulin Polymerization Inhibition Assay

Halting tubulin polymerization consequently disrupts the microtubule structure of the cell, and more importantly, microtubule function, thereby resulting in the induction of cellular apoptosis [40,41]. Tubulin polymerization inhibition has been established as a promising drug target for the development of novel treatments for cancers [42]. To demonstrate the cytotoxic activity shown by the synthesized *p*-vanillin Schiff base molecule

4g, a further experiment for the β-tubulin polymerization inhibition percent in the MCF-7 cells was performed at a concentration equal to its IC_{50} value. Col, a reference antimitotic drug, was also tested as a positive control compound. The suppression activity in this experiment was reported as the percent of β-tubulin polymerization inhibition. This experiment demonstrated that *p*-vanillin Schiff base **4g** revealed promising β-tubulin polymerization inhibition activity when compared to colchicine (Figure 2). The *p*-vanillin Schiff base produced 81.69% β-tubulin polymerization suppression compared with Col (88.92%). The observed cytotoxic activity of the *p*-vanillin Schiff base may be due to the potential β-tubulin polymerization inhibition activity.

Table 1. Cytotoxicity results of the tested Schiff base–TMB hybrids **3** and **4a–i** against the MCF-7 cells and normal breast cell line MCF-10A. Data expressed as the mean ± SD.

Comp No.	IC_{50} Value (μM)	
	MCF-7	MCF-10A
3	12.10 ± 0.95	NT
4a	6.20 ± 0.51	NT
4b	4.74 ± 0.47	NT
4c	18.64 ± 0.99	NT
4d	13.69 ± 0.89	NT
4e	24.02 ± 0.91	NT
4f	4.01 ± 0.25	NT
4g	2.28 ± 0.18	26.84 ± 0.32
4h	9.37 ± 0.56	NT
4i	102.09 ± 1.19	NT
Col	5.74 ± 0.21	31.15 ± 0.18

NT; not tested.

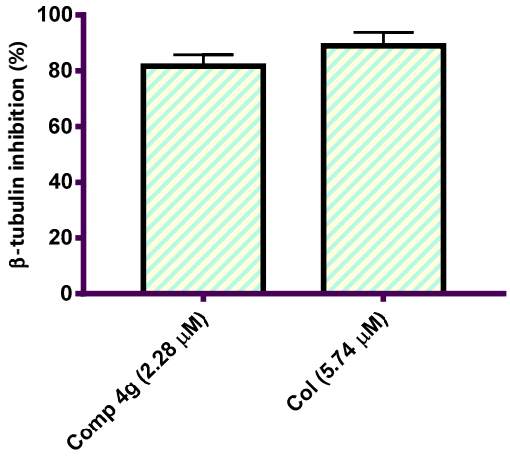

Figure 2. Graphical representation of the β-tubulin polymerization inhibition percentage in the MCF-7 cells after treatment with *p*-vanillin Schiff base **4g** and Col at their IC_{50} values (μM).

2.2.3. Cell Cycle Analysis

Tubulin–microtubule dynamics plays a vital role in regulating cellular division, proliferation, and cell survival [43]. Tubulin assembly inhibitors have shown efficacy in disrupting different cell cycle phases leading to cell cycle arrest and cellular apoptosis [44]. To prove that *p*-vanillin Schiff base **4g** can hijack the cell cycle, DNA flow cytometric analysis was carried out to detect the DNA content after exposing the MCF-7 cells to the IC_{50} concentration of *p*-vanillin Schiff base **4g** for 48 h. As shown in Figure 3, a cytometric profile of the stained DNA after the administration of *p*-vanillin Schiff base **4g** at its IC_{50} concentration caused an increase in the percent of G2/M phase in the MCF-7 cells compared with the untreated control. Specifically, an increase (34.78%) was detected in the *p*-vanillin Schiff base **4g** treated MCF-7 cells compared to the DMSO control (10.73%).

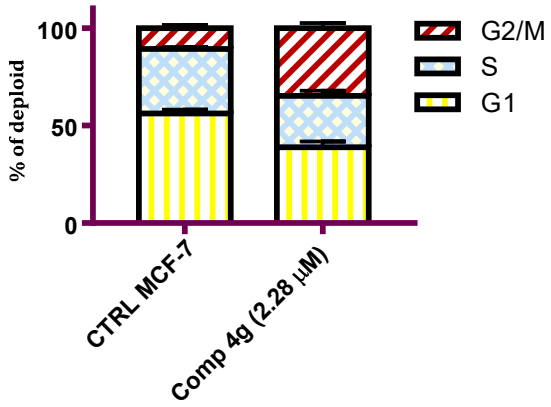

Figure 3. Flow cytometric analysis of the MCF-7 cells after the administration of the *p*-vanillin Schiff base **4g** at its IC_{50} concentration for 48 h. Each data point represents the mean of two independent experiments.

2.2.4. Apoptosis Staining Assay

Apoptosis plays a crucial role in normal tissue homeostasis in mature organisms [45]. The inhibition of apoptosis can contribute to the growth and development of cancer, so apoptosis induction in cancer cells might generate beneficial effects in cancer chemotherapy [46]. In the present experiment, fluorochrome Annexin V/PI staining analysis was carried out to study the effect of *p*-vanillin Schiff base **4g** regarding the ratio of early and late apoptosis in the MCF-7 cells following exposure to the IC_{50} concentration of the titled compound for 48 h. As shown in Figure 4, it was observed that the *p*-vanillin Schiff base **4g** increased the apoptotic cell percentages at both the early and late levels in the MCF-7 cell line compared with the DMSO control. The percentage of the early and late apoptotic cells was increased by 7.71- and 17.27-fold compared with the DMSO control. Therefore, *p*-vanillin Schiff base **4g** can be regarded as an inducer of apoptosis in the MCF-7 breast cancer cell line.

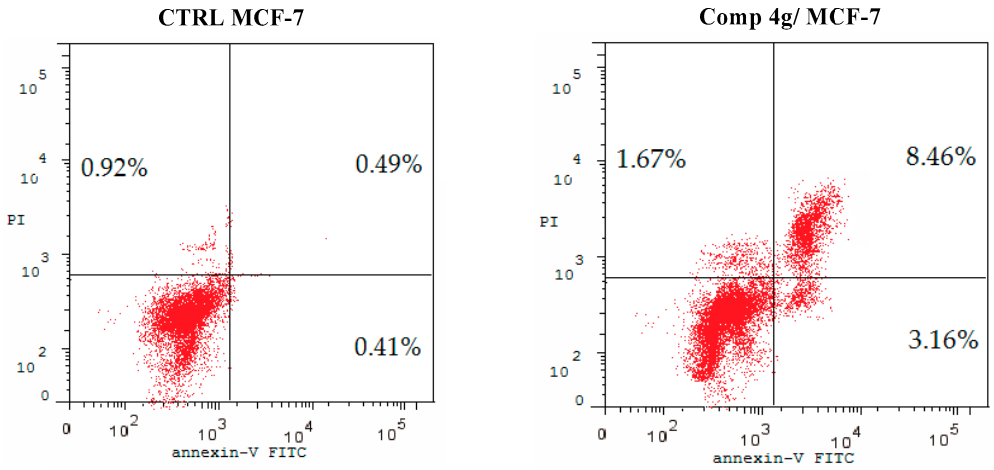

Figure 4. Proportion of apoptotic cells in the MCF-7 cells after 48 h following treatment with the IC_{50} value of *p*-vanillin Schiff base **4g** compared with the control untreated MCF-7 cells.

2.2.5. Quantitative Real-Time PCR: MCF-7 Breast Cancer Cells Express mRNA for Human p53, Bax, and Bcl-2

Increased production of the Bcl-2 protein and the inactivation of p53 and Bax occur very commonly in human cancers, which renders the cells resistant to the induction of apoptosis [47]. Molecular controls regulating the apoptosis process might ultimately generate more effective treatments for cancer [48]. In these experiments, qRT-PCR was used to assess the effect of *p*-vanillin Schiff base **4g** on the expression levels of p53, Bax, and Bcl-2

mRNA after exposure to the IC_{50} concentration of the titled compound **4g** for 48 h. GAPDH was utilized as the quality control amplicon to ensure consistent amplification between samples and fold changes. The results of these experiments declared that the mRNA levels of p53 and Bax were greatly increased after treatment with the IC_{50} concentration of *p*-vanillin Schiff base **4g** compared with the DMSO control. Meanwhile, the expression level of Bcl-2 was decreased compared with the untreated control. The data indicated that *p*-vanillin Schiff base **4g** upregulated p53 expression level by 5.21-fold higher than the untreated control (Figure 5A). Similarly, *p*-vanillin Schiff base **4g** increased the Bax level by 4.35-fold more than the DMSO control (Figure 5B). This upregulation in the p53 and Bax levels may be due to the DNA damage effect of the tested Schiff base molecule. On the other hand, the data showed a decrease in the Bcl-2 level by 0.22-fold less than the untreated control (Figure 5C). The data obtained from the qRT-PCR expression support the previous findings that Schiff base **4g** is a potent cytotoxic agent and triggers apoptotic induction in MCF-7 cells as a secondary effect to β-tubulin polymerization inhibition.

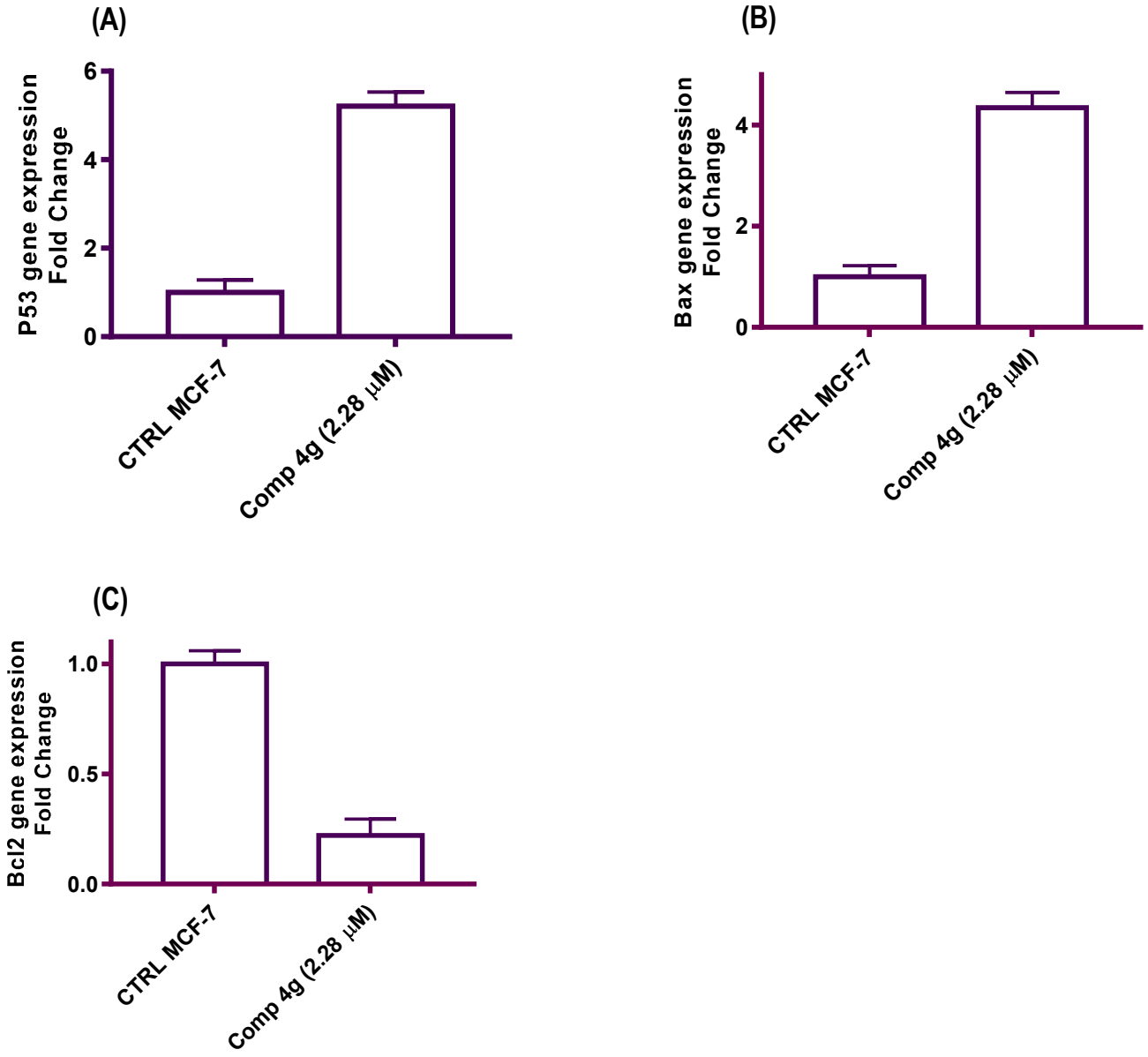

Figure 5. A diagram illustrated the effects of the IC_{50} *p*-vanillin Schiff base **4g** on the p53, Bax, and Bcl-2 mRNA expression levels in the MCF-7 cell line.

2.3. Molecular Docking Study

A molecular docking study was conducted to obtain a better understanding of the molecular behavior of *p*-vanillin Schiff base **4g**, which showed excellent activity in the tubulin inhibition assay. Molecular docking was carried out for the binding pocket in the tubulin active site (PDB ID: 1SA0) to predict the binding affinity of the synthesized *p*-vanillin Schiff base **4g** as a tubulin polymerization inhibitor using MOE 2015 software. The ability of *p*-vanillin Schiff base **4g** to interact with the key amino acids rationalizes its potential activity, as indicated by its docking score and docking pattern. As can be shown in Figure 6, compound **4g** interacted by its OH group of the *p*-vanillin moiety as the H-bond donor with the key amino acid Asn 228. As an H-bond acceptor, compound **4g** interacted with its methoxy oxygen of the *p*-vanillin moiety with Asn 206. The methoxy group of the TMB moiety interacted as the H-bond acceptor with the key amino acid Asn 101. Additionally, the hydrophobic side chain of Tyr 224 interacted hydrophobically with the phenyl ring of the *p*-vanillin moiety. Furthermore, the hydrophobicity of *p*-vanillin Schiff base **4g** led to a docking score of −23.66 kcal/mol.

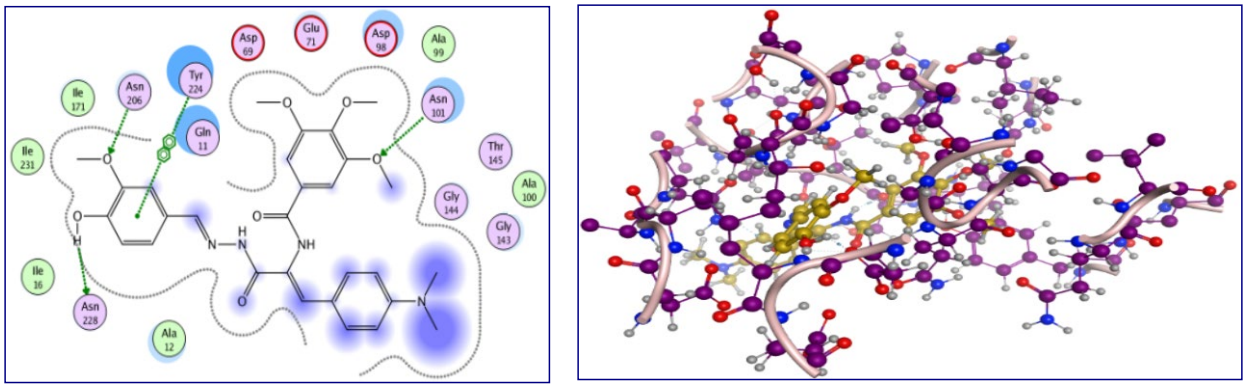

Figure 6. The 2D and 3D interactions of *p*-vanillin Schiff base **4g** with the amino acids of the tubulin active site.

3. Conclusions

A set of new hybrid molecules containing Schiff base and 3,4,5-trimethoxybenzamide moieties were designed and synthesized. The structures of the constructed Schiff base–trimethoxybenzamide hybrids were confirmed by ^{1}H-NMR and ^{13}C-NMR spectroscopic studies as well as elemental microanalysis. All of the target compounds were screened for their in vitro cytotoxic activity. Among them, the *p*-vanillin Schiff base **4g** showed good antiproliferative activity against the MCF-7 cells with an IC_{50} value of 2.28 µM compared with colchicine as the reference compound. Consistent with its antiproliferative activity, the cytotoxic activity of the tested Schiff base hybrids correlated to β-tubulin polymerization inhibition where *p*-vanillin Schiff base **4g** was a potent β-tubulin polymerization inhibitor compared to colchicine. Additionally, the cell cycle flow cytometric assay revealed that the *p*-vanillin Schiff base hybrid **4g** induced cellular cycle arrest at the G2/M phase of the MCF-7 cells. Moreover, the Schiff base hybrid **4g** is a potent apoptotic agent where the 4-hydroxy-3-methoxybenzylidene hydrazinyl molecule **4g** induced a high affinity for Annexin V and showed a percent apoptosis of 13.29% compared with the percent apoptosis of 1.82% for the control untreated MCF-7 cells. The qRT-PCR measurements for p53 and the cellular death modulators (Bax and Bcl-2) indicated that *p*-vanillin Schiff base **4g** triggers apoptosis induction via upregulation of the p53 and Bax mRNA expression level and downregulation of the expression of Bcl-2. Interestingly, the molecular docking study of *p*-vanillin Schiff base hybrid **4g** with the tubulin active site revealed that this molecule could bind nicely to the binding pocket of the tubulin active site, which led us to rationalize the importance of the *p*-vanillin group in holding the molecule by extra hydrogen bonds and justifies the experimental findings.

4. Experimental

4.1. Chemistry

4.1.1. General

To elucidate the chemical structures of the prepared Schiff base–TMB hybrids **3** and **4a–i**, the melting points, ^{1}H-NMR, ^{13}C-NMR, and elemental analysis were carried out. Section 4.1.1 provides the experimental details.

4.1.2. General Method for the Synthesis of (*Z*)-*N*-(1-(4-(Dimethylamino)phenyl)-3-hydrazinyl-3-oxoprop-1-en-2-yl)-3,4,5-trimethoxybenzamide (**2**)

A mixture of equimolar amounts of the 3,4,5-trimethoxybezamido ethyl ester derivative **(*Z*)-1** (12.85 g, 0.03 mol) and hydrazine hydrate in absolute ethanol (30 mL) was heated to reflux for 4 h and then left to cool at room temperature. The precipitate formed was filtered off and crystallized from aqueous ethanol (70%), affording the pure hydrazide product **(*Z*)-2**.

White powder, yield: 9.70 g, 78%; mp 190–192 °C. ^{1}H-NMR (400 MHz, DMSO-d_6) δ: 9.75 (s, 1H, NH), 9.28 (s, 1H, NH), 7.44 (d, *J* = 8.8 Hz, 2H, ArH), 7.40 (s, 2H, ArH), 7.16 (s, 1H, olefinic CH), 6.67 (d, *J* = 8.9 Hz, 2H, ArH), 4.34 (s, 2H, NH_2), 3.87 (s, 6H, $-2OCH_3$), 3.75 (s, 3H, $-OCH_3$), 2.91 (s, 6H, $-2CH_3$) ppm. ^{13}C-NMR (100 MHz, DMSO-d_6) δ: 165.69, 165.52, 152.96, 150.88, 140.64, 131.48, 130.44, 129.63, 124.78, 121.99, 112.12, 106.06, 60.56, 56.51, 40.15 ppm. Anal. Calcd. for $C_{21}H_{26}N_4O_5$ (414.45): C, 60.86; H, 6.32; N, 13.52. Found: C, 60.92; H, 6.35; N, 13.47.

4.1.3. General Procedure for the Synthesis of Schiff Bases **3** and **4a–i**

To a mixture of the hydrazide **(*Z*)-2** (0.50 g. 0.0012 mol) and furfural or the respective aromatic aldehyde (0.0012 mol) in absolute ethanol (20 mL), glacial acetic acid (15 drops) was added. The mixture was heated to reflux for 6–8 h. The obtained solid residue was filtered off while hot, washed with pure ethanol, and dried under vacuum to afford the objective molecules **3** and **4a–i**.

N-((*Z*)-1-(4-(Dimethylamino)phenyl)-3-((*E*)-2-(furan-2-ylmethylene)hydrazinyl)-3-oxoprop-1-en-2-yl)-3,4,5-trimethoxybenzamide (**3**)

Pale yellow powder, yield: 0.41 g, 69%; mp 239–241 °C. ^{1}H-NMR (400 MHz, DMSO-d_6) δ: 11.42 (s, 1H, NH), 9.87 (s, 1H, NH), 8.32 (s, 1H, CH=N), 7.83 (s, 1H, Furan-H), 7.50 (d, *J* = 8.6 Hz, 2H, ArH), 7.42 (s, 2H, ArH), 7.15 (s, 1H, olefinic CH), 6.87 (d, *J* = 3.3 Hz, 1H Furan-H), 6.71 (d, *J* = 8.6 Hz, 2H, ArH), 6.65–6.60 (m, 1H Furan-H), 3.87 (s, 6H, $-2OCH_3$), 3.75 (s, 3H, $-OCH_3$), 2.94 (s, 6H, $-2CH_3$) ppm. ^{13}C-NMR (100 MHz, DMSO-d_6) δ: 165.60, 162.94, 153.08, 151.05, 150.19, 145.39, 140.82, 131.75, 131.03, 129.27, 125.05, 121.74, 117.53, 113.33, 112.60, 112.14, 106.00, 60.59, 56.55, 40.14 ppm. Anal. Calcd. for $C_{26}H_{28}N_4O_6$ (492.52): C, 63.40; H, 5.73; N, 11.38. Found: C, 63.29; H, 5.79; N, 11.46.

N-((*Z*)-1-(4-(Dimethylamino)phenyl)-3-((*E*)-2-(2-hydroxybenzylidene)hydrazinyl)-3-oxoprop-1-en-2-yl)-3,4,5-trimethoxybenzamide (**4a**)

Yellow powder, yield: 0.42 g, 68%; mp 251–253 °C. ^{1}H-NMR (400 MHz, DMSO-d_6) δ: 11.76 (s, 1H, OH), 11.47 (s, 1H, NH), 9.92 (s, 1H, NH), 8.60 (s, 1H, CH=N), 7.52 (d, *J* = 8.8 Hz, 2H, ArH), 7.47 (d, *J* = 7.8 Hz, 1H, ArH), 7.44 (s, 2H, ArH), 7.29 (t, *J* = 7.7 Hz, 1H, ArH), 7.23 (s, 1H, olefinic CH), 6.92 (t, *J* = 8.7 Hz, 2H, ArH), 6.72 (d, *J* = 8.6 Hz, 2H, ArH), 3.88 (s, 6H, $-2OCH_3$), 3.76 (s, 3H, $-OCH_3$), 2.95 (s, 6H, $-2CH_3$) ppm. ^{13}C-NMR (100 MHz, DMSO-d_6) δ: 165.68, 162.75, 157.92, 153.10, 151.15, 148.19, 140.87, 131.87, 131.62, 131.54, 130.11, 129.21, 124.41, 121.61, 119.73, 119.18, 116.86, 112.14, 106.02, 60.60, 56.56, 40.13 ppm. Anal. Calcd. for $C_{28}H_{30}N_4O_6$ (518.56): C, 64.85; H, 5.83; N, 10.80. Found: C, 65.03; H, 5.74; N, 10.72.

N-((*Z*)-1-(4-(Dimethylamino)phenyl)-3-((*E*)-2-(4-hydroxybenzylidene)hydrazinyl)-3-oxoprop-1-en-2-yl)-3,4,5-trimethoxybenzamide (**4b**)

White powder, yield: 0.47 g, 75%; mp 260–262 °C. ^{1}H-NMR (400 MHz, DMSO-d_6) δ: 11.25 (s, 1H, NH), 9.88 (s, 1H, OH), 9.84 (s, 1H, NH), 8.31 (s, 1H, CH=N), 7.51 (t, *J* = 8.7 Hz, 4H, ArH), 7.42 (s, 2H, ArH), 7.14 (s, 1H, olefinic CH), 6.83 (d, *J* = 7.8 Hz, 2H, ArH), 6.71 (d, *J* = 8.6 Hz, 2H, ArH), 3.87 (s, 6H, −2OCH_3), 3.75 (s, 3H, −OCH_3), 2.94 (s, 6H, −2CH_3) ppm. ^{13}C-NMR (100 MHz, DMSO-d_6) δ: 165.59, 162.61, 159.62, 153.07, 150.98, 147.60, 140.79, 131.68, 130.69, 129.33, 129.08, 126.06, 125.24, 121.88, 116.12, 112.14, 105.99, 60.58, 56.55, 40.02 ppm. Anal. Calcd. for $C_{28}H_{30}N_4O_6$ (518.56): C, 64.85; H, 5.83; N, 10.80. Found: C, 64.95; H, 5.88; N, 10.71.

N-((*Z*)-3-((*E*)-2-(4-(Dimethylamino)benzylidene)hydrazinyl)-1-(4-(dimethylamino)phenyl)-3-oxoprop-1-en-2-yl)-3,4,5-trimethoxybenzamide (**4c**)

Orange powder, yield: 0.48 g, 73%; mp 263–265 °C. ^{1}H-NMR (400 MHz, DMSO-d_6) δ: 11.16 (s, 1H, NH), 9.84 (s, 1H, NH), 8.27 (s, 1H, CH=N), 7.51 (d, *J* = 4.5 Hz, 2H, ArH), 7.49 (d, *J* = 4.7 Hz, 2H, ArH), 7.42 (s, 2H, ArH), 7.14 (s, 1H, olefinic CH), 6.76 (d, *J* = 8.5 Hz, 2H, ArH), 6.70 (d, *J* = 9.0 Hz, 2H, ArH), 3.87 (s, 6H, −2OCH_3), 3.75 (s, 3H, −OCH_3), 2.97 (s, 6H, −2CH_3), 2.93 (s, 6H, −2CH_3) ppm. ^{13}C-NMR (100 MHz, DMSO-d_6) δ: 165.67, 162.52, 153.07, 151.82, 150.95, 148.18, 140.79, 131.65, 130.49, 129.38, 128.68, 125.42, 122.41, 121.93, 112.31, 112.14, 106.00, 60.58, 56.55, 40.26, 40.16 ppm. Anal. Calcd. for $C_{30}H_{35}N_5O_5$ (545.63): C, 66.04; H, 6.47; N, 12.84. Found: C, 65.92; H, 6.58; N, 12.98.

N-((*Z*)-1-(4-(Dimethylamino)phenyl)-3-((*E*)-2-(4-methylbenzylidene)hydrazinyl)-3-oxoprop-1-en-2-yl)-3,4,5-trimethoxybenzamide (**4d**)

White powder, yield: 0.47 g, 76%; mp 221–223 °C. ^{1}H-NMR (400 MHz, DMSO-d_6) δ: 11.41 (s, 1H, NH), 9.88 (s, 1H, NH), 8.38 (s, 1H, CH=N), 7.59 (d, *J* = 7.9 Hz, 2H, ArH), 7.51 (d, *J* = 8.9 Hz, 2H, ArH), 7.42 (s, 2H, ArH), 7.26 (d, *J* = 7.1 Hz, 2H, ArH), 7.16 (s, 1H, olefinic CH), 6.71 (d, *J* = 9.0 Hz, 2H, ArH), 3.87 (s, 6H, −2OCH_3), 3.75 (s, 3H, −OCH_3), 2.94 (s, 6H, −2CH_3), 2.34 (s, 3H, −CH_3) ppm. ^{13}C-NMR (100 MHz, DMSO-d_6) δ: 165.58, 162.89, 153.08, 151.02, 147.24, 140.81, 140.01, 132.36, 131.73, 130.84, 129.88, 129.29, 127.34, 125.16, 121.83, 112.14, 105.99, 60.58, 56.55, 40.15, 21.49 ppm. Anal. Calcd. for $C_{29}H_{32}N_4O_5$ (516.59): C, 67.43; H, 6.24; N, 10.85. Found: C, 67.36; H, 6.18; N, 10.93.

N-((*Z*)-1-(4-(Dimethylamino)phenyl)-3-((*E*)-2-(4-methoxybenzylidene)hydrazinyl)-3-oxoprop-1-en-2-yl)-3,4,5-trimethoxybenzamide (**4e**)

Pale yellow powder, yield: 0.35 g, 54%; mp 229–231 °C. ^{1}H-NMR (400 MHz, DMSO-d_6) δ: 11.33 (s, 1H, NH), 9.85 (s, 1H, NH), 8.35 (s, 1H, CH=N), 7.63 (d, *J* = 8.6 Hz, 2H, ArH), 7.49 (d, *J* = 8.9 Hz, 2H, ArH), 7.41 (s, 2H, ArH), 7.14 (s, 1H, olefinic CH), 7.01 (d, *J* = 8.0 Hz, 2H, ArH), 6.70 (d, *J* = 9.0 Hz, 2H, ArH), 3.86 (s, 6H, −2OCH_3), 3.80 (s, 3H, −OCH_3), 3.74 (s, 3H, −OCH_3), 2.93 (s, 6H, −2CH_3) ppm. ^{13}C-NMR (100 MHz, DMSO-d_6) δ: 165.58, 162.78, 161.09, 153.07, 151.00, 147.16, 140.80, 131.71, 130.73, 129.31, 128.92, 127.64, 125.26, 121.83, 114.78, 112.14, 105.99, 60.58, 56.55, 55.75, 40.15 ppm. Anal. Calcd. for $C_{29}H_{32}N_4O_6$ (532.59): C, 65.40; H, 6.06; N, 10.52. Found: C, 65.48; H, 5.95; N, 10.55.

N-((*Z*)-1-(4-(Dimethylamino)phenyl)-3-((*E*)-2-(2-hydroxy-3-methoxybenzylidene)hydrazinyl)-3-oxoprop-1-en-2-yl)-3,4,5-trimethoxybenzamide (**4f**)

Pale yellow powder, yield: 0.43 g, 66%; mp 262–264 °C. ^{1}H-NMR (400 MHz, DMSO-d_6) δ: 11.74 (s, 1H, NH), 11.24 (s, 1H, OH), 9.91 (s, 1H, NH), 8.60 (s, 1H, CH=N), 7.52 (d, *J* = 8.9 Hz, 2H, ArH), 7.44 (s, 2H, ArH), 7.23 (s, 1H, olefinic CH), 7.07 (d, *J* = 7.7 Hz, 1H, ArH), 7.02 (d, *J* = 7.9 Hz, 1H, ArH), 6.86 (t, *J* = 7.9 Hz, 1H, ArH), 6.72 (d, *J* = 9.0 Hz, 2H, ArH), 3.88 (s, 6H, −2OCH_3), 3.82 (s, 3H, −OCH_3), 3.76 (s, 3H, −OCH_3), 2.94 (s, 6H, −2CH_3) ppm. ^{13}C-NMR (100 MHz, DMSO-d_6) δ: 165.68, 163.11, 162.72, 153.10, 151.15, 148.37, 148.14, 147.64, 140.86, 131.86, 131.59, 129.21, 124.46, 121.63, 121.52, 119.40, 114.12, 112.14, 106.02,

60.60, 56.56, 56.26, 40.13 ppm. Anal. Calcd. for $C_{29}H_{32}N_4O_7$ (548.59): C, 63.49; H, 5.88; N, 10.21. Found: C, 63.55; H, 6.02; N, 10.13.

N-((*Z*)-1-(4-(Dimethylamino)phenyl)-3-((*E*)-2-(4-hydroxy-3-methoxybenzylidene)hydrazinyl)-3-oxoprop-1-en-2-yl)-3,4,5-trimethoxybenzamide (**4g**)

Yellow powder, yield: 0.47 g, 71%; mp 203–205 °C. ^{1}H-NMR (400 MHz, DMSO-d_6) δ: 11.29 (s, 1H, NH), 9.86 (s, 1H, NH), 9.29 (s, 1H, OH), 8.27 (s, 1H, CH=N), 7.50 (d, *J* = 8.9 Hz, 2H, ArH), 7.43 (s, 2H, ArH), 7.29–7.22 (m, 1H, ArH), 7.15 (s, 1H, olefinic CH), 7.02 (dd, *J* = 8.3, 1.7 Hz, 1H, ArH), 6.96 (d, *J* = 8.3 Hz, 1H, ArH), 6.70 (d, *J* = 9.0 Hz, 2H, ArH), 3.87 (s, 6H, −2OCH$_3$), 3.81 (s, 3H, −OCH$_3$), 3.76 (s, 3H, −OCH$_3$), 2.94 (s, 6H, −2CH$_3$) ppm. ^{13}C-NMR (100 MHz, DMSO-d_6) δ: 165.61, 162.75, 153.08, 151.00, 150.04, 147.46, 147.32, 140.81, 131.71, 130.74, 129.31, 127.93, 125.24, 121.84, 120.45, 112.68, 112.35, 112.14, 106.00, 60.58, 56.55, 56.03, 40.15 ppm. Anal. Calcd. for $C_{29}H_{32}N_4O_7$ (548.59): C, 63.49; H, 5.88; N, 10.21. Found: C, 63.58; H, 5.93; N, 10.14.

N-((*Z*)-3-((*E*)-2-(3,5-Dimethoxybenzylidene)hydrazinyl)-1-(4-(dimethylamino)phenyl)-3-oxoprop-1-en-2-yl)-3,4,5-trimethoxybenzamide (**4h**)

Pale yellow powder, yield: 0.43 g, 64%; mp 198–200 °C. ^{1}H-NMR (400 MHz, DMSO-d_6) δ: 11.50 (s, 1H, NH), 9.89 (s, 1H, NH), 8.34 (s, 1H, CH=N), 7.51 (d, *J* = 8.9 Hz, 2H, ArH), 7.42 (s, 2H, ArH), 7.15 (s, 1H, olefinic CH), 6.88–6.80 (m, 2H, ArH), 6.71 (d, *J* = 9.0 Hz, 2H, ArH), 6.56 (s, 1H, ArH), 3.87 (s, 6H, −2OCH$_3$), 3.79 (s, 6H, −2OCH$_3$), 3.75 (s, 3H, −OCH$_3$), 2.94 (s, 6H, −2CH$_3$) ppm. ^{13}C-NMR (100 MHz, DMSO-d_6) δ: 165.62, 163.03, 161.13, 153.08, 151.04, 147.10, 140.81, 137.10, 131.76, 130.90, 129.27, 125.18, 121.74, 112.14, 105.98, 105.14, 102.41, 60.58, 56.54, 55.77, 40.14 ppm. Anal. Calcd. for $C_{30}H_{34}N_4O_7$ (562.61): C, 64.04; H, 6.09; N, 9.96. Found: C, 63.91; H, 5.97; N, 10.05.

N-((*Z*)-1-(4-(Dimethylamino)phenyl)-3-oxo-3-((*E*)-2-(3,4,5-trimethoxybenzylidene)hydrazinyl)prop-1-en-2-yl)-3,4,5-trimethoxybenzamide (**4i**)

Yellow powder, yield: 0.45 g, 63%; mp 195–197 °C. ^{1}H-NMR (400 MHz, DMSO-d_6) δ 11.47 (s, 1H, NH), 9.89 (s, 1H, NH), 8.35 (s, 1H, CH=N), 7.51 (d, *J* = 8.7 Hz, 2H, ArH), 7.42 (s, 2H, ArH), 7.13 (s, 1H, olefinic CH), 6.99 (s, 2H, ArH), 6.72 (d, *J* = 8.9 Hz, 2H, ArH), 3.87 (s, 6H, −2OCH$_3$), 3.83 (s, 6H, −2OCH$_3$), 3.75 (s, 3H, −OCH$_3$), 3.71 (s, 3H, −OCH$_3$), 2.94 (s, 6H, −2CH$_3$) ppm. ^{13}C-NMR (100 MHz, DMSO-d_6) δ: 165.65, 162.97, 153.64, 153.07, 151.03, 147.3, 140.81, 139.46, 131.75, 130.77, 130.58, 129.27, 125.24, 121.76, 112.14, 105.98, 104.58, 60.58, 56.54, 56.39, 40.15 ppm. Anal. Calcd. for $C_{31}H_{36}N_4O_8$ (592.64): C, 62.83; H, 6.12; N, 9.45. Found: C, 63.04; H, 6.24; N, 9.36.

4.2. Biological Studies

4.2.1. MTT Cytotoxicity Assay

The effect of the Schiff base–TMB hybrids **3** and **4a–i** on the breast cancer (MCF-7) cell line was examined using the MTT colorimetric test (see Supplementary Materials Section S4.2.1).

4.2.2. β-Tubulin Polymerization Assay

To investigate the hybrids' cytotoxic potential, the β-tubulin polymerization assay of *p*-vanillin Schiff base–TMB hybrid **4g** was performed (see Supplementary Materials Section S4.2.2).

4.2.3. Cell Cycle Analysis

FACS analysis was used to analyze the cellular cycle in the MCF-7 cells in accordance with the manufacturer's recommendations (see Supplemental Materials Section S4.2.3).

4.2.4. Annexin V/FITC Staining Assay

According to the manufacturer's instructions, FACS analysis was used to perform a double staining analysis with Annexin and FITC on MCF-7 cells (see Supplemental Materials Section S4.2.4).

4.2.5. Effect on p53, Bax, and Bcl-2 Expression Levels

p53, Bax, and Bcl-2, which are apoptotic markers, were assessed in the MCF-7 cells using qRT-PCR in accordance with the manufacturer's instructions (see Supplementary Materials Section S4.2.5).

Supplementary Materials: The following supporting information can be downloaded at: https://www.mdpi.com/article/10.3390/sym15030609/s1, **Figure S1:** ^{1}H-NMR spectrum of compound **2**, **Figure S2:** ^{13}C-NMR spectrum of compound **2**, **Figure S3:** ^{1}H-NMR spectrum of compound **3**, **Figure S4:** ^{13}C-NMR spectrum of compound **3**, **Figure S5:** ^{1}H-NMR spectrum of compound **4a**, **Figure S6:** ^{13}C-NMR spectrum of compound **4a**, **Figure S7:** ^{1}H-NMR spectrum of compound **4b**, **Figure S8:** ^{13}C-NMR spectrum of compound **4b**, **Figure S9:** ^{1}H-NMR spectrum of compound **4c**, **Figure S10:** ^{13}C-NMR spectrum of compound **4c**, **Figure S11:** ^{1}H-NMR spectrum of compound **4d**, **Figure S12:** ^{13}C-NMR spectrum of compound **4d**, **Figure S13:** ^{1}H-NMR spectrum of compound **4e**, **Figure S14:** ^{13}C-NMR spectrum of compound **4e**, **Figure S15:** ^{1}H-NMR spectrum of compound **4f**, **Figure S16:** ^{13}C-NMR spectrum of compound **4f**, **Figure S17:** ^{1}H-NMR spectrum of compound **4g**, **Figure S18:** ^{13}C-NMR spectrum of compound **4g**, **Figure S19:** ^{1}H-NMR spectrum of compound **4h**, **Figure S20:** ^{13}C-NMR spectrum of compound **4h**, **Figure S21:** ^{1}H-NMR spectrum of compound **4i**, **Figure S22:** ^{13}C-NMR spectrum of compound **4i**, **Figure S23:** Compound 4g induce G2/M phase disturbance in MCF-7 cells, **Table S1:** The primer sequences for Real Time PCR assay.

Funding: This research received no external funding.

Data Availability Statement: Not applicable.

Conflicts of Interest: The authors declare no conflict of interest.

References

1. Łukasiewicz, S.; Czeczelewski, M.; Forma, A.; Baj, J.; Sitarz, R.; Stanisławek, A. Breast Cancer—Epidemiology, Risk Factors, Classification, Prognostic Markers, and Current Treatment Strategies—An Updated Review. *Cancers* **2021**, *13*, 4287. [CrossRef] [PubMed]
2. Forooshani, M.K.; Scarpitta, R.; Fanelli, G.; Miccoli, M.; Naccarato, A.; Scatena, C. Is it time to consider the Androgen receptor as a therapeutic target in breast cancer? *Anti-Cancer Agents Med. Chem.* **2022**, *22*, 775. [CrossRef] [PubMed]
3. Mann, R.M.; Athanasiou, A.; Baltzer, P.; Camps-Herrero, J.; Clauser, P.; Fallenberg, E.; Forrai, G.; Fuchsjäger, M.; Helbich, T.; Killburn-Toppin, F.; et al. Breast cancer screening in women with extremely dense breasts recommendations of the European Society of Breast Imaging (EUSOBI). *Eur. Radiol.* **2022**, *32*, 4036. [CrossRef] [PubMed]
4. Kumar-Sinha, C.; Chinnaiyan, A.M. Defining cancer growth beyond the mitotic index. *Nat. Cell Biol.* **2022**, *24*, 285. [CrossRef]
5. Novais, P.; Silva, P.; Amorim, I.; Bousbaa, H. Second-generation antimitotics in cancer clinical trials. *Pharmaceutics* **2021**, *13*, 1011. [CrossRef]
6. Shuai, W.; Wang, G.; Zhang, Y.; Bu, F.; Zhang, S.; Miller, D.; Li, W.; Ouyang, L.; Wang, Y. Recent Progress on Tubulin Inhibitors with Dual Targeting Capabilities for Cancer Therapy. *J. Med. Chem.* **2021**, *64*, 7963. [CrossRef]
7. Ebenezer, O.; Shapi, M.; Tuszynski, J.A. A Review of the Recent Developments of Molecular Hybrids Targeting Tubulin Polymerization. *Int. J. Mol. Sci.* **2022**, *23*, 4001. [CrossRef]
8. Jaunky, D.B.; Larocque, K.; Husser, M.; Liu, J.; Forgione, P.; Piekny, A. Characterization of a recently synthesized microtubule-targeting compound that disrupts mitotic spindle poles in human cells. *Sci. Rep.* **2021**, *11*, 23665. [CrossRef]
9. Huang, L.; Peng, Y.; Tao, X.; Ding, X.; Li, R.; Jiang, Y.; Zuo, W. Microtubule Organization Is Essential for Maintaining Cellular Morphology and Function. *Oxidative Med. Cell. Longev.* **2022**, *2022*, 1623181. [CrossRef]
10. Spiliotis, E.T.; Nakos, K. Cellular functions of actin- and microtubule-associated septins. *Curr. Biol.* **2021**, *31*, R651. [CrossRef]
11. Khwaja, S.; Kumar, K.; Das, R.; Negi, A.S. Microtubule associated proteins as targets for anticancer drug development. *Bioorg. Chem.* **2021**, *116*, 105320. [CrossRef] [PubMed]
12. Best, R.L.; LaPointe, N.; Azarenko, O.; Miller, H.; Genualdi, C.; Chih, S.; Shen, B.-Q.; Jordan, M.; Wilson, L.; Feinstein, S.; et al. Microtubule and tubulin binding and regulation of microtubule dynamics by the antibody drug conjugate (ADC) payload, monomethyl auristatin E (MMAE): Mechanistic insights into MMAE ADC peripheral neuropathy. *Toxicol. Appl. Pharmacol.* **2021**, *421*, 115534. [CrossRef]

13. Romagnoli, R.; Oliva, P.; Salvador, M.; Manfredini, S.; Padroni, C.; Brancale, A.; Ferla, S.; Hamel, E.; Ronca, R.; Maccarinelli, F.; et al. A facile synthesis of diaryl pyrroles led to the discovery of potent colchicine site antimitotic agents. *Eur. J. Med. Chem.* **2021**, *214*, 113229. [CrossRef] [PubMed]
14. Mousset, C.; Giraud, A.; Provot, O.; Hamze, A.; Bignon, J.; Liu, J.-M.; Thoret, S.; Dubois, J.; Brion, J.-D.; Alami, M. Synthesis and antitumor activity of benzils related to combretastatin A-4. *Bioorg. Med. Chem. Lett.* **2008**, *18*, 3266. [CrossRef] [PubMed]
15. Zheng, J.; Deng, L.; Chen, M.; Xiao, X.; Xiao, S.; Guo, C.; Xiao, G.; Bai, L.; Ye, W.; Zhang, D.; et al. Elaboration of thorough simplified vinca alkaloids as antimitotic agents based on pharmacophore similarity. *Eur. J. Med. Chem.* **2013**, *65*, 158. [CrossRef]
16. Piekuś-Słomka, N.; Mikstacka, R.; Ronowicz, J.; Sobiak, S. Hybrid cis-stilbene molecules: Novel anticancer agents. *Int. J. Mol. Sci.* **2019**, *20*, 1300. [CrossRef]
17. Bukhari, S.N.A.; Zakaria, M.; Munir, M.; Ahmad, N.; Elsherif, M.; Badr, R.; Hassan, A.; Almaaty, A.; Zaki, I. Design, Synthesis, In Vitro Biological Activity Evaluation and Stabilized Nanostructured Lipid Carrier Formulation of Newly Synthesized Schiff Bases-Based TMP Moieties. *Pharmaceuticals* **2022**, *15*, 679. [CrossRef]
18. McLoughlin, E.C.; O'Boyle, N.M. Colchicine-Binding Site Inhibitors from Chemistry to Clinic: A Review. *Pharmaceuticals* **2020**, *13*, 8. [CrossRef]
19. Bertheloot, D.; Latz, E.; Franklin, B.S. Necroptosis, pyroptosis and apoptosis: An intricate game of cell death. *Cell. Mol. Immunol.* **2021**, *18*, 1106. [CrossRef]
20. Azarbarzin, S.; Hosseinpour-Feizi, M.; Khojasteh, S.B.; Baradaran, B.; Safaralizadeh, R. MicroRNA-383-5p restrains the proliferation and migration of breast cancer cells and promotes apoptosis via inhibition of PD-L1. *Life Sci.* **2021**, *267*, 118939. [CrossRef]
21. Zuo, Y.; Zhang, C.-Z.; Ren, Q.; Chen, Y.; Li, X.; Yang, J.-R.; Li, H.-X.; Tang, W.-T.; Ho, H.-M.; Sun, C.; et al. Activation of mitochondrial-associated apoptosis signaling pathway and inhibition of PI3K/Akt/mTOR signaling pathway by voacamine suppress breast cancer progression. *Phytomedicine* **2022**, *99*, 154015. [CrossRef] [PubMed]
22. Placzek, W.J.; Wei, J.; Kitada, S.; Zhai, D.; Reed, J.; Pellecchia, M. A survey of the anti-apoptotic Bcl-2 subfamily expression in cancer types provides a platform to predict the efficacy of Bcl-2 antagonists in cancer therapy. *Cell Death Dis.* **2010**, *1*, e40. [CrossRef] [PubMed]
23. Zaki, I.; Moustafa, A.; Beshay, B.; Masoud, R.; Elbastawesy, M.; Abourehab, M.; Zakaria, M.Y. Design and synthesis of new trimethoxylphenyl-linked combretastatin analogues loaded on diamond nanoparticles as a panel for ameliorated solubility and antiproliferative activity. *J. Enzym. Inhib. Med. Chem.* **2022**, *37*, 2679. [CrossRef] [PubMed]
24. Zhang, Z.; Bai, L.; Hou, L.; Deng, H.; Luan, S.; Liu, D.; Huang, M.; Zhao, L. Trends in targeting Bcl-2 anti-apoptotic proteins for cancer treatment. *Eur. J. Med. Chem.* **2022**, *232*, 114184. [CrossRef] [PubMed]
25. Al-Warhi, T.; Aldhahrani, A.; Althobaiti, F.; Fayad, E.; Ali, O.A.; Albogami, S.; Almaaty, A.A.; Khedr, A.; Bukhari, S.; Zaki, I. Design, Synthesis and Cytotoxic Activity Evaluation of Newly Synthesized Amides-Based TMP Moiety as Potential Anticancer Agents over HepG2 Cells. *Molecules* **2022**, *27*, 3960. [CrossRef]
26. Tadele, K.T.; Tsega, T.W. Schiff Bases and their metal complexes as potential anticancer candidates: A review of recent works. *Anti-Cancer Agents Med. Chem.* **2019**, *19*, 1786. [CrossRef]
27. Howsaui, H.B.; Basaleh, A.; Abdellattif, M.; Hassan, W.; Hussien, M.A. Synthesis, Structural Investigations, Molecular Docking, and Anticancer Activity of Some Novel Schiff Bases and Their Uranyl Complexes. *Biomolecules* **2021**, *11*, 1138. [CrossRef]
28. Shekhar, S.; Khan, A.; Sharma, S.; Sharma, B.; Sarkar, A. Schiff base metallodrugs in antimicrobial and anticancer chemotherapy applications: A comprehensive review. *Emergent Mater.* **2022**, *5*, 279. [CrossRef]
29. Uddin, N.; Rashid, F.; Ali, S.; Tirmizi, S.; Ahmad, I.; Zaib, S.; Zubair, M.; Diaconescu, P.; Tahir, M.; Iqbal, J.; et al. Synthesis, characterization, and anticancer activity of Schiff bases. *J. Biomol. Struct. Dyn.* **2020**, *38*, 3246. [CrossRef]
30. Medarde, M.; Maya, A.; Pérez-Melero, C. Naphthalene Combretastatin Analogues: Synthesis, Cytotoxicity and Antitubulin Activity. *J. Enzyme Inhib. Med. Chem.* **2004**, *19*, 521. [CrossRef]
31. Iacopetta, D.; Rosano, C.; Puoci, F.; Parisi, O.; Saturnino, C.; Caruso, A.; Longo, P.; Ceramella, J.; Malzert-Fréon, A.; Dallemagne, P.; et al. Multifaceted properties of 1,4-dimethylcarbazoles: Focus on trimethoxybenzamide and trimethoxyphenylurea derivatives as novel human topoisomerase II inhibitors. *Eur. J. Pharm. Sci.* **2017**, *96*, 263. [CrossRef] [PubMed]
32. Piplani, P.; Sharma, M.; Mehta, P.; Malik, R. N-(4-Hydroxyphenyl)-3,4,5-trimethoxybenzamide derivatives as potential memory enhancers: Synthesis, biological evaluation and molecular simulation studies. *J. Biomol. Struct. Dyn.* **2018**, *36*, 1867. [CrossRef] [PubMed]
33. Panno, A.; Sinicropi, M.; Caruso, A.; El-Kashef, H.; Lancelot, J.-C.; Aubert, G.; Lesnard, A.; Cresteil, T.; Rault, S. New Trimethoxybenzamides and Trimethoxyphenylureas Derived from Dimethylcarbazole as Cytotoxic Agents. Part I. *J. Heterocycl. Chem.* **2014**, *51*, E294. [CrossRef]
34. Li, Q.; Jian, X.-E.; Chen, Z.-R.; Chen, L.; Huo, X.-S.; Li, Z.-H.; You, W.-W.; Rao, J.-J.; Zhao, P.-L. Synthesis and biological evaluation of benzofuran-based 3,4,5-trimethoxybenzamide derivatives as novel tubulin polymerization inhibitors. *Bioorg. Chem.* **2020**, *102*, 104076. [CrossRef]
35. Jiménez, C.; Ellahioui, Y.; Álvarez, R.; Aramburu, L.; Riesco, A.; González, M.; Vicente, A.; Dahdouh, A.; Mansour, A.I.; Jiménez, C.; et al. Exploring the size adaptability of the B ring binding zone of the colchicine site of tubulin with para-nitrogen substituted isocombretastatins. *Eur. J. Med. Chem.* **2015**, *100*, 210. [CrossRef]

36. Lara, R.; Millán, G.; Moreno, M.; Lalinde, E.; Alfaro-Arnedo, E.; López, I.; Larráyoz, I.; Pichel, J.G. Investigation on Optical and Biological Properties of 2-(4-Dimethylaminophenyl)benzothiazole Based Cycloplatinated Complexes. *Chem. Eur. J.* **2021**, *27*, 15757. [CrossRef]
37. Zaki, I.; Masoud, R.; Hamoud, M.; Ali, O.; Abualnaja, M.; Fayad, E.; Almaaty, A.; Elnaghia, L.K. Design, synthesis and cytotoxicity screening of new synthesized pyrimidine-5-carbonitrile derivatives showing marked apoptotic effect. *J. Mol. Struct.* **2022**, *1259*, 132749. [CrossRef]
38. Al-Warhi, T.; Abualnaja, M.; Ali, O.A.; Althobaiti, F.; Alharthi, F.; Elsaid, F.; Shati, A.; Fayad, E.; Elghareeb, D.; Almaaty, A.A.; et al. Synthesis and Biological Activity Screening of Newly Synthesized Trimethoxyphenyl-Based Analogues as Potential Anticancer Agents. *Molecules* **2022**, *27*, 4621. [CrossRef]
39. Al-Warhi, T.; Alqahtani, L.; Abualnaja, M.; Beigh, S.; Ali, O.A.; Elsaid, F.; Shati, A.; Saleem, R.; Maghrabi, A.; Alharthi, A.; et al. Design, Synthesis, and In Vitro Antiproliferative Screening of New Hydrazone Derivatives Containing cis-(4-Chlorostyryl) Amide Moiety. *Symmetry* **2022**, *14*, 2457. [CrossRef]
40. Boichuk, S.; Galembikova, A.; Syuzov, K.; Dunaev, P.; Bikinieva, F.; Aukhadieva, A.; Zykova, S.; Igidov, N.; Gankova, K.; Novikova, M.; et al. The Design, Synthesis, and Biological Activities of Pyrrole-Based Carboxamides: The Novel Tubulin Inhibitors Targeting the Colchicine-Binding Site. *Molecules* **2021**, *26*, 5780. [CrossRef]
41. Haider, K.; Rahaman, S.; Yar, M.; Kamal, A. Tubulin inhibitors as novel anticancer agents: An overview on patents (2013–2018). *Expert Opin. Ther. Patents* **2019**, *29*, 623. [CrossRef]
42. Guo, K.; Ma, X.; Li, J.; Zhang, C.; Wu, L. Recent advances in combretastatin A-4 codrugs for cancer therapy. *Eur. J. Med. Chem.* **2022**, *241*, 114660. [CrossRef] [PubMed]
43. Borys, F.; Joachimiak, E.; Krawczyk, H.; Fabczak, H. Intrinsic and Extrinsic Factors Affecting Microtubule Dynamics in Normal and Cancer Cells. *Molecules* **2020**, *25*, 3705. [CrossRef] [PubMed]
44. Srivastava, A.; Fatima, K.; Fatima, E.; Singh, A.; Singh, A.; Shukla, A.; Luqman, S.; Shanker, K.; Chanda, D.; Khan, F.; et al. Fluorinated benzylidene indanone exhibits antiproliferative activity through modulation of microtubule dynamics and antiangiogenic activity. *Eur. J. Pharm. Sci.* **2020**, *154*, 105513. [CrossRef] [PubMed]
45. Henson, P.M.; Hume, D.A. Apoptotic cell removal in development and tissue homeostasis. *Trends Immunol.* **2006**, *27*, 244. [CrossRef] [PubMed]
46. Piskorz, W.M.; Cechowska-Pasko, M. Senescence of Tumor Cells in Anticancer Therapy—Beneficial and Detrimental Effects. *Int. J. Mol. Sci.* **2022**, *23*, 11082. [CrossRef] [PubMed]
47. Adams, J.M.; Cory, S. The BCL-2 arbiters of apoptosis and their growing role as cancer targets. *Cell Death Differ.* **2018**, *25*, 27. [CrossRef]
48. Dadsena, S.; King, L.; García-Sáez, A.J. Apoptosis regulation at the mitochondria membrane level. *Biochim. Biophys. Acta Biomembr.* **2021**, *1863*, 183716. [CrossRef]